JOURNAL MATERIALS SCIENCE 14 (1979) 2384–2390

# Measurement of the effect of microstructural variations on the energy of (Co, Ni) – $Cr_{23}C_6$ eutectic

G. ZAMBELLI, W. KURZ
*Department of Materials Engineering, Federal Institute of Technology, Lausanne, Switzerland*

The measurement of sector areas of load–deflection curves in the Tattersall–Tappin test permits evaluation of the fracture energy dissipated by the microstructure during crack propagation. This method has been applied to the oriented pseudo-binary (Co, Ni)–$Cr_{23}C_6$ eutectic alloys which exhibit an irregular, continuous network of brittle carbides within a ductile (Co, Ni, Cr) phase. In spite of the complexity of the microstructure analysed, the method proposed for measuring the fracture energy seems to be capable of revealing the fundamental influence of the size, volume and properties of the phases on the fracture energy of the alloys. An increase in the fracture energy for crack propagation has been observed with: (a) an increase in the size (spacing) of the phases for a constant volume fraction; (b) an increase in the volume fraction of the ductile phase; (c) a progressive increase of the Ni content of the alloy (for values above 5 wt % Ni); the highest values being observed for the pure ternary system: Co–$Cr_{23}C_6$ and Ni–$Cr_{23}C_6$.

## 1. Introduction

The eutectic alloy, (Co, Ni)–$Cr_{23}C_6$, has interesting mechanical properties at elevated temperatures, but is brittle at ambient temperatures [1]. Its structure consists of an irregular arrangement of branched, $Cr_{23}C_6$ carbides [2] forming a geometrically isotropic network distributed throughout a ductile Co, Ni, Cr–solid solution (Fig. 1). The factors influencing the fracture energy of such a heterogeneous structure are not well understood. In the present work, the effect of modifying the volume and size of the brittle phase on the energy of crack propagation, without varying the type (shape) of microstructure, is studied. The irregular inhomogeneous structure of the eutectic makes it impossible to meet the requirements for $K_{Ic}$ toughness measurement procedures described in the ASTM standards [3], $K_{Ic}$ measures being valid for materials with homogeneous elastic properties. For this reason, another type of test was used.

An attractive method is the Tattersall–Tappin (T–T) test, which gives stable crack growth, following initiation [4], due to the geometry of the notch of the specimen, and the conditions of controlled displacement.

The fracture work measured in the T–T test gives the energy dissipated irreversibly due to the combined influences of the microstructure, and of the geometry of the specimen. By changing the volume and size of the brittle phase the composition of the ductile phase, and measuring the resultant variation of the fracture energy, it is possible to isolate the individual effect of these parameters on the fracture mechanism.

## 2. Method

The fracture energy of a two-phase alloy is the sum of the surface free energy of the brittle phase, the energy associated with plastic flow of the ductile phase and other energies arising from processes occurring in the microstructure during fracture e.g. interface debonding. In order to measure the fracture energy, a test was chosen which allows slow, stable crack growth. Tattersall and Tappin

 0022–2461/79/102384–07 $02.70/0 

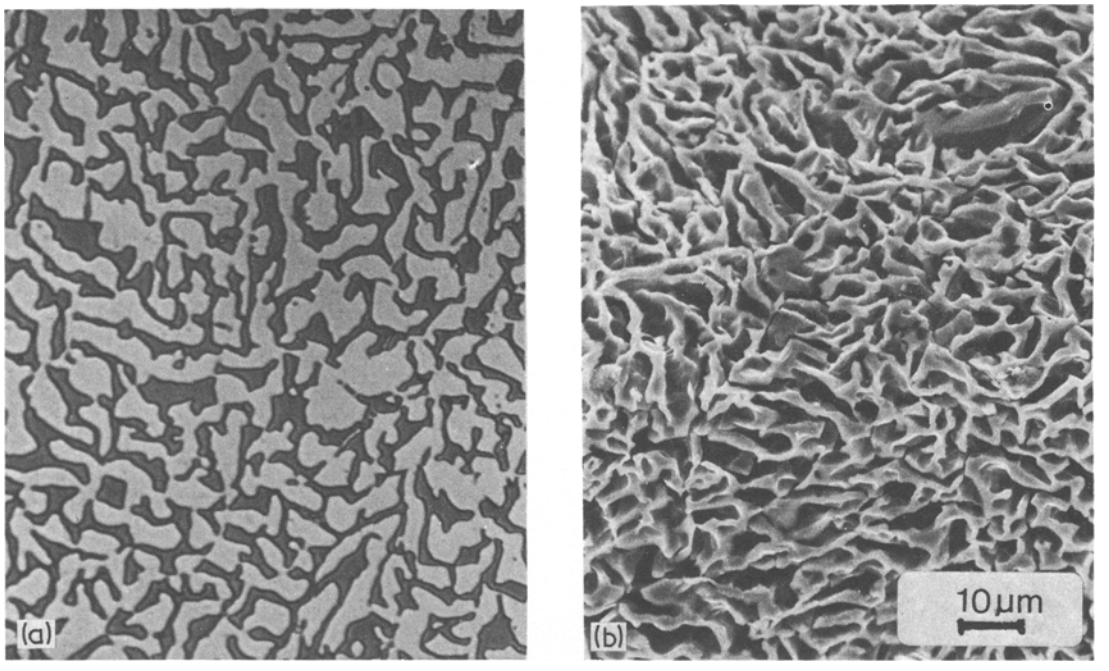


*Figure 1* Microstructure of oriented alloy 15. Growth rate, $V = 6.7\,\mu m\,sec^{-1}$, temperature gradient $= 7.5\,K\,mm^{-1}$. (a) transverse section, (b) $Cr_{23}C_6$ carbide network (deep etch).

[4] and Nakayama [5] have used square, 3-point bending test specimens having a triangular cross-section at the central crack plane (Fig. 2). The crack starts at the apex of the triangle and continually widens as it propagates through the specimen. If the test conditions are chosen correctly, the crack grows in a quasi-static manner (controlled fracture). Under these conditions, it is known that the energy per unit area, $G_c$, required to propagate the crack, may be obtained from the load–deflection curve [6]. This quantity, which is often called the fracture toughness, is equal to $2\gamma$, where $\gamma$ is the energy associated with the creation of fracture surface. $G_c$ has been evaluated in the following way (Fig. 2):

The increase in fracture area, $\Delta A$, is given by the following relationship for the triangular shape of the fracture surface:

$$\Delta A = (a_2 - a_1)(a_1 + a_2)B/2W. \qquad (1)$$

In the present tests, in order to emphasize the fact that the energy for crack propagation per unit area $\Delta A$, is measured, we use the designation, $R^p$, instead of $G_c$. The fracture energy, $\bar{R}^p$, is taken to be the average of the $R_n^p$ values for five sectors. These sectors are drawn on the experimentally determined $P$–$\delta$ curve (Fig. 3) so as to correspond to equal, apparent fracture areas of $\Delta A = 1\,mm^2$. This procedure thus fixes a series of values, $a_n$, for the crack length. This latter quantity was measured directly, and also deduced from compliance measurements made during the test.

The compliance calibrations for the T–T specimens were made using steel specimens and the results corrected for the difference in elastic moduli between the steel and the material tested [1]. This standard calibration also gave an experimental check on the position of the crack at different stages of propagation. In order to avoid the apex effect, the crack length, $a_1 = 1.5\,mm$, was arbitrarily chosen to mark the first sector.

A hard screw type tensile testing machine, and a 100 kN load cell were used in order to minimize displacements in the loading system. The deflection, $\delta$, was recorded by means of an electromechanical transducer (LVDT) placed in the axis of load application. The cross-head speed, $4.2\,\mu m\,sec^{-1}$, was the same in all of the experiments. By keeping to the same specimen geometry in T–T tests made on different microstructures, the variation, $\Delta R^p$, measured as shown in Fig. 3, gives the contribution of the change in microstructure to the fracture energy for crack propagation.

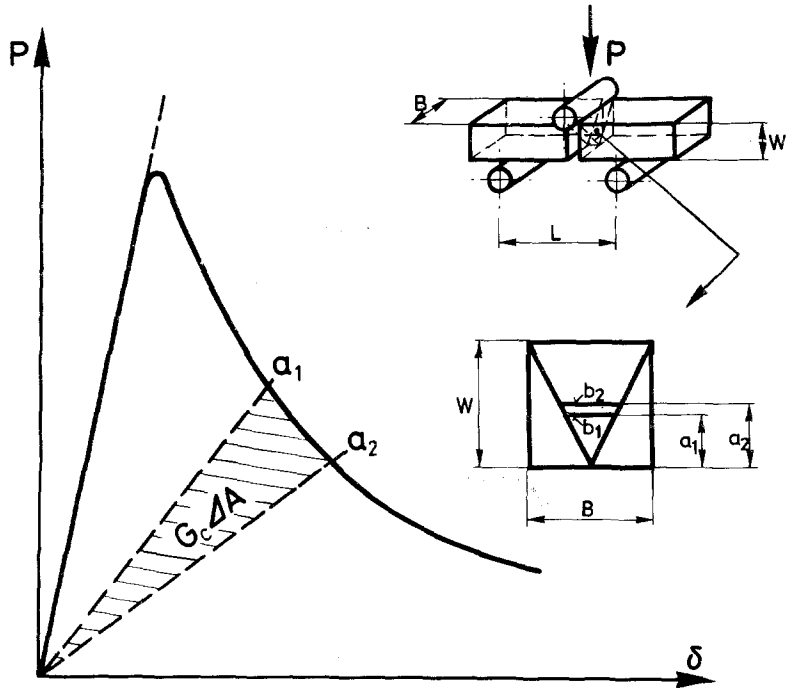


*Figure 2* Load–deflection curve of T–T specimen ($B = 5$ mm, $W = 4$ mm, $L = 20$ mm).

The energy, $R_n^p$, dissipated during propagation of the crack from $a_n$ to $a_{n+1}$, is given by:

$$R_n^p = \frac{U_{(n)}}{2q\Delta A_{(n)}} \quad (2)$$

where $U_{(n)}$ is the energy corresponding to the sector $n$ ($0 - a_1 - a_2$ for sector $n = 1$ in Fig. 3), and $q$ is a roughness factor. This factor is the ratio of the real surface area of the fracture surface to the projected surface area. It is estimated from microscopic observations of the profiles of sections cut perpendicularly to the fracture plane. The factor, $q$, is used in order to characterise the contribution from changes of fracture path length which arise from variations in carbide network geometry. This contribution to the fracture energy $R_n^p$ must be distinguished from that arising from the fracture microprocesses: plastic deformation and multiple cracking.

## 3. Results

A study of the role, of the size and volume of the phases in determining the fracture energy, was carried out on alloy 15 (Table I). The carbides in this alloy, even when observed on metallographic sections, can be considered as connected particles (Fig. 4).

A linear erosion technique [7], programmed on an automatic image analyser gave, from distribution curves, the mean free distance, $\lambda_d$, between carbides (equal to thickness of the ductile phase), the "thickness" of the carbides, $\lambda_c$, and the interphase spacing, $\lambda = \lambda_c + \lambda_d$ [8]. These parameters were varied by changing the growth rate during directional solidification [2].

A progressive decrease in carbide volume fraction was measured along the axis of the directionally solidified alloy 15. The decrease was most

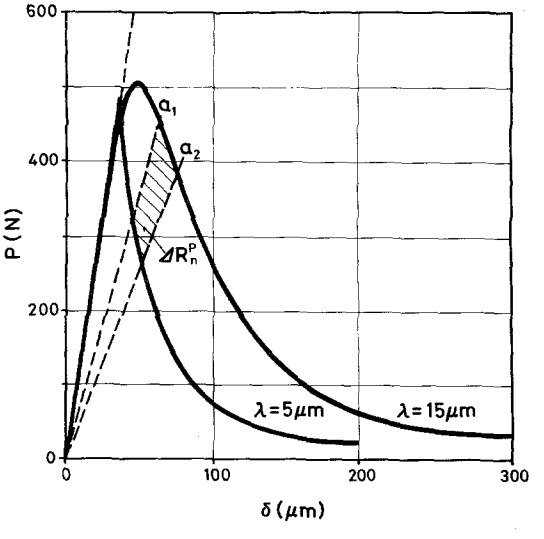


*Figure 3* Load–deflection curves for two interphase spacings of oriented alloy 15.

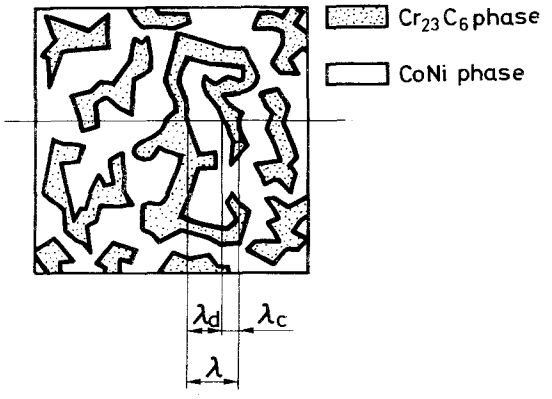


*Figure 4* Schematic of two phase structure of (Co, Ni) $Cr_{23}C_6$ alloys.

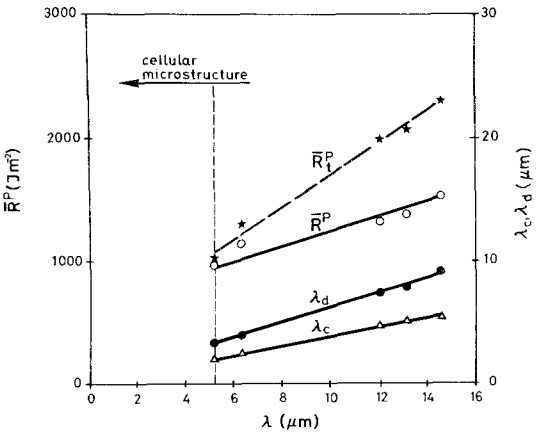


*Figure 5* Fracture energy, $\bar{R}^p$, mean free distance between carbides, $\lambda_d$, and "thickness" of carbides, $\lambda_c$, as a function of the interphase spacing, λ. Oriented alloy 15 ($V_d = 64\%$).

pronounced at low rates of solidification and this effect was attributed to a reaction between the alumina crucible and the constituents (Cr and C) of the alloys. Values of the carbide volume fraction were measured over the whole transverse section beneath the fracture plane. These measurements give an average value which included the effect of radial variations caused by the oxidation reaction between the crucible and the alloy. In order to isolate the effect of the scale of the microstructure on fracture, tests were made on specimens having the same volume fraction of the two phases ($V = 64\%$ Co, Ni). These specimens were maintained in the liquid state for various times before directional solidification so that on varying the growth rate, the overall reaction time with the crucible was constant. The triangular cross-section determining the fracture path is transverse to the growth direction of the specimen. Fig. 3 gives $P$–$\delta$ curves for two extreme values (5 μm and 15 μm) of the interphase spacing, λ. These limits are fixed by those conditions of unidirectional solidification which lead to similar microstructures, and avoid cell formation at the solid–liquid interface.

The variation of the average value of the fracture energy $\bar{R}^p$, as a function of the interphase spacing, λ, is shown in Fig. 5. The value of $\bar{R}^p$ increases from 950 J m$^{-2}$ ($\lambda = 5\,\mu$m) to 1550 J m$^{-2}$ ($\lambda = 15\,\mu$m). The mean free distance between carbides, $\lambda_d$, and the carbide thickness, $\lambda_c$, increase proportionally, with the ratio $\lambda_c/\lambda_d$ (= 0.56) staying constant, since the volume fraction is constant. $\bar{R}^p_t$ gives the fracture energy without the fracture surface roughness correction.

## 3.1. Volume fraction

For equal values of the mean free distance, $\lambda_d$, of the carbides, an increase in volume fraction, $V_d$, of the ductile phase led to an increase in dissipated fracture energy, $\bar{R}^p$ (Fig. 6). The values, $\bar{R}^p$, are given for $\lambda_d = 8\,\mu$m and $\lambda_d = 5\,\mu$m. The load–deflection curves show an increase in the maximum load when the volume fraction, $V_d$, increases (Fig. 7).

## 3.2. Composition

While maintaining the chromium and carbon content, and the growth rate ($V = 6.7\,\mu$m sec$^{-1}$) constant, the amounts of nickel and cobalt, in (Co, Ni)–$Cr_{23}C_6$, were varied as shown in Table I.

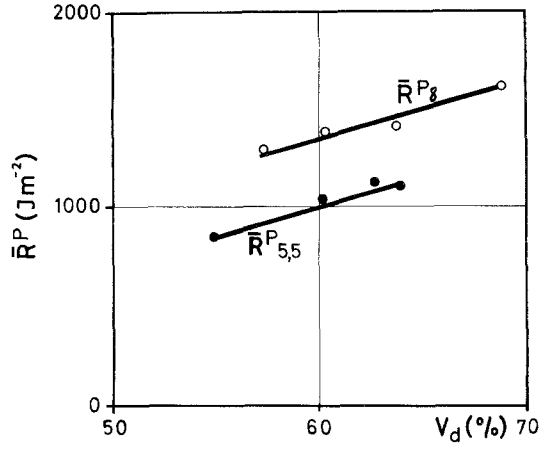


*Figure 6* Fracture energy, $\bar{R}^p$, for microstructures with $\lambda_d = 8\,\mu$m and 5.5 μm as a function of the volume fraction, $V_d$, of the ductile (Co, Ni) phase.

TABLE I Pseudo-binary eutectics in the Co–Ni–Cr–C system

| Alloy | | $\frac{Ni}{Co+Cr+Ni}$ | $\frac{Ni}{Co+Ni}$ | Alloy composition (wt%) | | | | $V_d$ |
|---|---|---|---|---|---|---|---|---|
| | | | | Co | Ni | Cr | C | (%) |
| 0 | Co–$Cr_{23}C_6$ | 0 | 0 | 49 | – | 49 | 2 | 58 |
| 5 | (Co, Ni5) $Cr_{23}C_6$ | 0.07 | 0.10 | 45 | 5 | 48 | 2 | 64 |
| 10 | (Co, Ni10) $Cr_{23}C_6$ | 0.12 | 0.20 | 40 | 10 | 48 | 2 | 64 |
| 15 | (Co, Ni15) $Cr_{23}C_6$ | 0.20 | 0.30 | 35.1 | 15 | 48 | 1.9 | 64 |
| 25 | (Co, Ni25) $Cr_{23}C_6$ | 0.32 | 0.50 | 25 | 25 | 48 | 2 | 64 |
| 40 | (Co, Ni40) $Cr_{23}C_6$ | 0.52 | 0.80 | 10 | 40 | 48 | 2 | 64 |
| 46 | Ni–$Cr_{23}C_6$ | 0.58 | 1 | – | 46.4 | 52 | 1.6 | 75 |

The characteristic microstructure of alloy 15 was maintained in all the alloys studied. Fig. 8 shows the fracture energy, $R^p$, as a function of the nickel content of the ductile phase (Co, Ni, Cr) for the alloys studied. A minimum value of $R^p = 750\ J\ m^{-2}$, was measured for alloy 5. Increase in the nickel concentration gives a proportional increase in $R^p$ up to a limit of 3000 $J\ m^{-2}$ for the Co-free ternary alloy 46 (Ni–$Cr_{23}C_6$). For the Ni-free alloy 0 i.e. the Co–$Cr_{23}C_6$ eutectic, the mean value of the fracture energy, $R^p$, was 2500 $J\ m^{-2}$. The scatter in the latter results can be ascribed to the irregularity of the structure due to the clustering of the fine carbide branches.

## 4. Discussion

Experimental studies of fracture paths in (Co, Ni)–$Cr_{23}C_6$ alloys showed that crack extension occurred preferentially within the carbide phase. However, crack tip blunting involving ductile ligaments of the Co, Ni phase could occur at discontinuities in the irregular carbide network. The $\bar{R}_n^p$ values are assumed, by definition, to be proportional to the fracture energy, $R_c$, of the carbide phase, and the energy, $R_m$, dissipated by fracture deformation of the ductile ligaments.

The variation of fracture energy, $\Delta\bar{R}_n^p$, measured for different interphase spacings and compositions, but always for the same type of microstructure, will be mainly dependent on the variation of the energy, $\Delta R_m$, dissipated by fracture mechanisms acting in the microstructure during propagation not allowing for the effect of change in fracture path (roughness correction). Thus, one is able to investigate the individual effects, of changes in microstructure, on the fracture energy.

The procedure of measuring the areas of sectors and thereby obtaining fracture data during crack

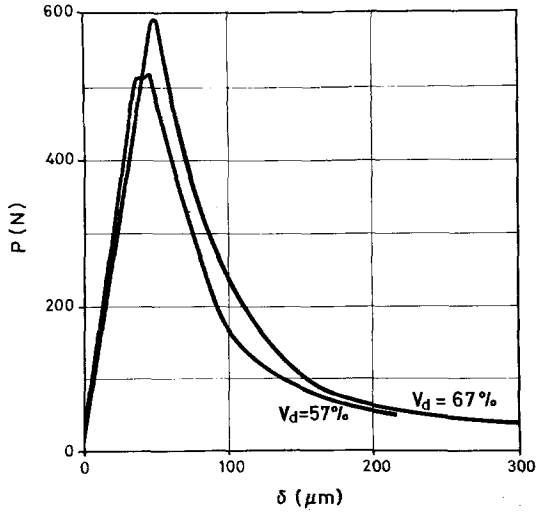


*Figure 7* Load–deflection curves for two volume fractions of ductile (Co, Ni, Cr) phase. Alloy 15, $\lambda_d = 8\ \mu m$.

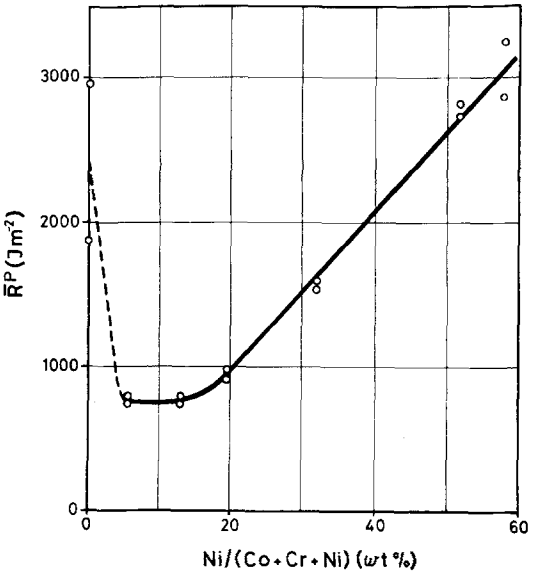


*Figure 8* The variation of the fracture energy, $\bar{R}^p$, as a function of the nickel content of the ductile phase. Eutectic oriented at $V = 6.7\ \mu m\ sec^{-1}$.

TABLE II $R^p$ values measured for 3 interphase spacings of alloy 15, and their standard deviation, $S$, compared with the work of fracture, $\gamma_F$, of Tattersall and Tappin [4]. Values given in J m$^{-2}$.

| $\gamma$ ($\mu$m) | $R_1^p$ | $R_2^p$ | $R_3^p$ | $R_4^p$ | $R_5^p$ | $\bar{R}^p$ | $S_{R_p}$ | $\gamma_F$ | $S_{\gamma_F}$ |
|---|---|---|---|---|---|---|---|---|---|
| 14.6 | 1493 | 1568 | 1548 | 1413 | 1700 | 154 | 106 | 1654 | 210 |
| 12.1 | 1266 | 1245 | 1460 | 1300 | 1375 | 1330 | 88 | 1485 | 195 |
| 5.2 | 1019 | 949 | 919 | 831 | 1114 | 966 | 106 | 1101 | 205 |

propagation has certain advantages over the traditional use of the T–T test. There, the total area under the load–deflection curve along with the cracked triangular tip area is used to obtain a "work of fracture". This has the disadvantage that there is a transition from plane stress conditions, at the apex of the triangle, to plane strain conditions after crack has grown some distance. Also, the machining of the triangular cross-section may lead to damaged carbides near the apex which then give a large difference in crack initiation. In addition, the stress conditions at the end of the test are less clearly defined.

This situation is clearly apparent in Table II which gives for instance, the values measured for $R^p_{(n)}$ and $\bar{R}^p$ in comparison with the normal Tattersall–Tappin (T–T) measures $\gamma_F$, for alloy 15. These results shown lower values for our method than those obtained in the normal T–T method. This is certainly due to those testing conditions limiting the normal T–T test. The standard deviation $\bar{S}^p_R$ is small in comparison with the values $S_{\gamma_F}$ for normal T–T tests.

In general, two types of load–deflection curves are observed (Fig. 9): Type A, in which the curves have the same slopes before crack propagation, has been observed for alloy 15 oriented at different rates ($\lambda$ variable), but with a constant volume fraction of the phases (compare Fig. 3). In the B-type behaviour (Fig. 9), the maximum loads, and the slopes of the curves, before crack propagation are different. The load–deflection curves recorded for alloy 15 in which a variation in volume fraction occurred, were of this type (Fig. 7).

Variation of the nickel and cobalt contents of the alloys gives different load–deflection curves. The ternary eutectic alloys Co–$Cr_{23}C_6$ and Ni–$Cr_{23}C_6$ show type B behaviour: the microstructure of the nickel-free alloy consists of a large quantity of small carbides and a relatively small amount of ductile (Co, Cr) phase. This would be expected to lead to a low fracture energy $\bar{R}^p$. The relatively large value of $\bar{R}^p$ measured must be attributed to the contribution of deformation processes during fracture of the (Co, Cr) phase [8]. For the cobalt-free alloy, the high $\bar{R}^p$ values measured are probably due to the high volume fraction, $V_d$, of the NiCr solid solution at the fracture surface.

When nickel is progressively substituted for cobalt in the quaternary (CoNi)–$Cr_{23}C_6$ eutectic alloys, an increase in fracture energy, $\bar{R}^p$, going from alloy 5 to alloy 40 has been observed (Fig. 8). The load–deflection curves for these alloys are of type A (Fig. 9). The values of the size parameters,

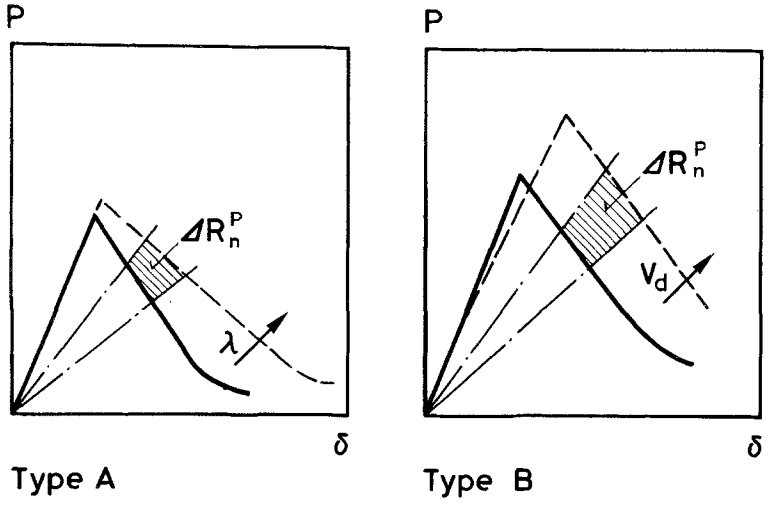


*Figure 9* Schematic load–deflection curves from T–T tests for alloys with different microstructures in oriented (Co, Ni)–$Cr_{23}C_6$ eutectic.

$\lambda_c$, $\lambda_d$ and $V_d$ which are constant within the limits of error, suggest that the change in fracture energy is due to variation in the toughness of the (Co, CrNi) phase.

In conclusion, the method proposed in this paper permits measurement of the influence of the microstructure, of two-phase alloys, on the fracture energy. The detailed fracture mechanisms are discussed elsewhere [9].

## Acknowledgements

The authors wish to thank Professor I. Finnie (University of California, Berkeley), Dr A. Kelly (University of Surrey), and Dr G. A. Cooper (Institute CERAC, Lausanne) for their helpful discussions during the study. This work is part of a project financed jointly by the "Kommission zur Förderung der wissenschaftlichen Forschung", Brown Boveri, Baden, and Sulzer Bros., Winterthur, Switzerland.

## References

1. E. R. THOMPSON and F. D. LEMKEY, "Composite Materials", Vol. 4, edited by L. J. Broutman, R. H. Krock (Academic Press, New York, 1974) p. 102.
2. G. ZAMBELLI and D. D. DOUBLE, *J. Mater. Sci.* **13** 1978) 534.
3. ASTM: E 399-74, Standard Test Method for Plane-strain Fracture Toughness of Metallic Materials (1974).
4. H. G. TATTERSALL and G. TAPPIN, *J. Mater. Sci.* **1** (1966) 296.
5. J. NAKAYAMA, *J. Amer. Ceram. Soc.* 48 (1965) 583.
6. I. FINNIE, "An Introduction to Fracture", Lecture notes (1977) EPF Lausanne, Switzerland.
7. G. ZAMBELLI, Sc. D. Thesis (1976), Ecole Polytechnique Fédérale de Lausanne, Switzerland.
8. L. REMY, F. LECROISEY, A. PINEAU, *Mém. Sci. Rev. Métall.* 7–8 (1973) 589.
9. G. ZAMBELLI and W. KURZ, to be published.

Received 12 December 1978 and accepted 23 March 1979.